GaAs/Indium Tin Oxide/Si Bonding Junctions for III-V-on-Si Hybrid Multijunction Cells With Low Series Resistance

Naoteru Shigekawa , *Member, IEEE*, Tomoya Hara, Tomoki Ogawa, Jianbo Liang, *Member, IEEE*, Takefumi Kamioka, *Member, IEEE*, Kenji Araki , *Member, IEEE*, and Masafumi Yamaguchi , *Life Member, IEEE*

Abstract—Effects of GaAs/indium tin oxide (ITO)/Si junctions on III-V-on-Si multijunction solar cells are examined by fabricating and characterizing InGaP/GaAs/ITO/Si triple-junction (3J) solar cells. The 3J cells are fabricated by evaporating $\approx$ 100-nm-thick ITO films on the surfaces of Si bottom cells and bonding the InGaP/GaAs double-junction (2J) subcells and the ITO films using surface-activated bonding technologies at room temperature. The current–voltage characteristics of 3J cells with p^+-GaAs/ITO/n^+-Si and n^+-GaAs/ITO/n^+-Si junctions are compared with those of an InGaP/GaAs/Si 3J cell. The parasitic resistance of the respective 3J cells is estimated by analyzing their characteristics in the dark. We find that the 3J cell with an n^+-GaAs/ITO/n^+-Si junction shows the lowest parasitic resistance, which is the origin of its lowest differential resistance at the open-circuit voltage and highest fill factor. This means that n^+-GaAs/ITO/n^+-Si junctions are promising for improving the performances of III-V-on-Si hybrid multijunction cells. The spectral response characteristics of these cells indicate that the thickness of the ITO films must be optimized.

Index Terms—Hybrid junctions, indium tin oxide (ITO), InGaP/GaAs/Si, multijunction solar cell fabrication, surface-activated bonding (SAB).

I. INTRODUCTION

MULTIJUNCTION solar cells fabricated by cascading subcells with different bandgaps have exhibited the highest conversion efficiencies among solar cell structures [1]. Proposed multijunction cells include AlGaAs/GaAs [2] and InGaP/(In)GaAs double-junction (2J) cells [3]–[6], InGaP/(In)GaAs/Ge [7] and InGaP/GaAs/InGaAs [8] triple-junction (3J) cells, and InGaP/GaAs/InGaAsP/InGaAs four-junction (4J) cells [9], [10]. Their excellent performance has

been demonstrated by integrating them with equipment for concentrating solar light. An efficiency of >46% at 508 suns was reported for a 4J cell [10].

For the purpose of realizing photovoltaics with high efficiencies and low costs [11], several authors fabricated III-V-on-Si multijunction cells by growing III-V subcells on Si-based bottom cells [12], [13]. Although III-V (sub) cells were successfully grown on Si by using GaAsP-graded buffer layers [14] or Ge/Si templates [15], [16], the performance of the obtained III-V cells was still limited because of the threading dislocations because of the difference in lattice constants between the III-V materials and Si [13].

For multijunction cell fabrication, an alternative to epitaxial growth is low-temperature wafer bonding, which makes it possible to stack foreign semiconductor materials with different crystal structures, lattice constants, and thermal expansion coefficients [17], [18]. Several types of bonding technologies such as conventional direct bonding [19], smart stack approach [20], and surface-activated bonding (SAB) [21]–[24] have been successfully applied for fabricating multijunction solar cells.

In SAB [25], the surfaces of substrates to be bonded are first irradiated by a fast atom beam (FAB) of Ar, which removes native oxide layers from the surfaces, or activates the surfaces. The substrates are then weighted at low temperatures so that they can be bonded to each other. Fabricated and characterized homojunctions and heterojunctions include Si/Si [25]–[27] Ge/Ge [28], Si/GaAs [29]–[32], Si/InP [33], Si/InGaP [34], Si/GaN [35], and Si/SiC [36], [37] junctions. We found that a junction made of p^+-GaAs and n^+-Si substrates and that made of n^+-GaAs and n^+-Si substrates exhibited a resistance of 0.13 [31] and 0.074 Ωcm^2 [32], respectively. We also fabricated n-on-p InGaP/Si 2J cells [22] and n-on-p InGaP/GaAs/Si 3J cells [23] by bonding lattice-matched III-V layers grown on GaAs substrates to Si bottom cells, removing the GaAs substrates, forming emitter and base contacts, performing mesa-etching, and depositing antireflection films. The bonding interfaces were made of p^+-GaAs and n^+-Si.

Because of the bandgaps of the respective subcells in InGaP/GaAs/Si 3J systems, there occurs mismatching in short-circuit currents among the subcells so the efficiencies of the 3J cells are limited when they are under air mass 1.5G solar irradiance. The impacts of this drawback were alleviated and an efficiency as high as >30% was achieved by using the

double-path configuration for the Si bottom cells and arranging the thickness of the III-V layers [24] or by replacing the GaAs middle cells with AlGaAs cells and optimizing passivation of both sides of the Si bottom cells [38]. Other proposed approaches for decreasing the impacts of the current mismatching include partially covering the Si bottom cells with the III-V upper subcells [39] and replacing a single subcell with two cascading subcells of the same materials (for example by replacing GaAs/Si 2J with GaAs/GaAs/Si 3J [40]).

The FAB irradiation is likely to induce damage, which acts as mid-gap states, on the surfaces of bonded substrates. An analysis based on the charge neutrality level model suggested that the mid-gap states cause a potential barrier at the bonding interfaces, which increases interface resistance [27]. However, the contribution of the potential barrier was suppressed by optimizing the bonding conditions, such as the bonding temperature and FAB energy [41]. In [41], a resistance of $< 3.6 \times 10^{-3} \ \Omega \text{cm}^2$ was reported for a junction of n^+-GaAs and n^+-Si substrates, which was much lower than a resistance obtained for an n^+-GaAs substrate/n^+-Si substrate junction in our group [32].

We estimated the resistance across the p^+-GaAs/n^+-Si bonding interface in actual 3J cells by characterizing cells with extra tap contacts connected to the p^+-GaAs and n^+-Si bonding layers [42]. The thickness of the n^+-Si bonding layers, which also worked as emitters of bottom cells, was ∼10 nm. The obtained resistance, several Ωcm^2, was much higher than the resistance of bonding interfaces made of p^+-GaAs and n^+-Si substrates fabricated using the same SAB conditions (0.13 Ωcm^2 as stated above [31]). The assumed reason for the difference in the resistance was that the impacts of potential barriers because of the FAB irradiation manifested themselves more apparently in junctions of thin bonding layers than in junctions made of heavily doped substrates. Irrespective of the origin, the obtained results imply that the resistance across the bonding interface should limit the characteristics of hybrid multijunction cells.

A practical solution for the higher resistance in the bonding interfaces of 3J cells might be provided by using conductive transparent oxides such as indium tin oxide (ITO) as bonding layers for Si bottom cells. Actually, ITO films have been widely utilized as top contacts in Si-based [43]–[45] and III-V-based [46] solar cells. They have also been used as intermediate layers in bonding n-InGaP and n-GaAs layers [47]. In [47], the temperature of the samples was raised to 650 °C during the bonding process. The bonding was reportedly achieved because of the diffusion of In atoms from the InGaP layers to the ITO films. We previously fabricated Si/ITO/Si junctions by bonding heavily doped Si substrates to ITO films deposited on other Si substrates [48]. In [48], we found that the electrical conduction across the Si/ITO bonding interfaces was degraded by annealing at temperatures higher than 400 °C. Consequently, in using ITO films as intermediate layers for III-V-on-Si multijunction cells, the bonding at lower temperatures is preferable so as to minimize the increase in the interface resistance because of heating.

We recently fabricated InGaP/GaAs/ITO/Si 3J cells and found that their performance is better than that of conventional InGaP/GaAs/Si 3J cells [49]. The change in performances was related to the lower differential resistance observed for 3J cells

with ITO intermediate layers. In this paper, as an extension to [49], we focus on the electrical properties of GaAs/ITO/Si junctions and highlight their impact on the characteristics of 3J cells. After briefly describing the process for depositing ITO films and the performance of 3J cells, we formulate a method for extracting the parasitic resistance, or the resistance that is not due to the intrinsic p–n junctions, from the measured current–voltage (I–V) characteristics of 3J cells. Then, we clarify the contribution of the ITO film to the resistance of their bonding interfaces. The optical properties of ITO film and its contribution to the spectral response of 3J cells are also examined.

II. EXPERIMENTS

A. Methods

ITO films were deposited on a glass plate and an n^+-Si (100) substrate using the plasma-evaporation without substrate heating. The impurity concentration of the n^+-Si substrate was $2.6 \times 10^{19} \ \text{cm}^{-3}$. The thickness of the ITO film was nominally 100 nm. The morphology of surfaces of ITO films deposited on n^+-Si (100) substrates was examined by atomic force microscopy (AFM). We also measured the transmittance of the ITO on a glass plate and the reflectance of the ITO on Si.

We also prepared p^+- and n^+-GaAs epi-layers by using MOVPE growth on p- and n-GaAs (100) substrates, respectively. The nominal impurity concentrations in the p^+-GaAs and n^+-GaAs epi-layers, N_A and N_D, were equally ∼$10^{19} \ \text{cm}^{-3}$. Both the p^+- and n^+-GaAs epi-layers were bonded to the ITO films on the n^+-Si substrates to form the p^+-GaAs/ITO/n^+-Si and n^+-GaAs/ITO/n^+-Si junctions. Ohmic contacts had been formed on the backsides of the respective substrates before bonding. The conditions in the bonding process were the same as those used in previous work [26], [27]. Note that, as in the process for fabricating 3J cells, the samples were not heated in the bonding process. The structural properties of interfaces were examined by scanning electron microscopy (SEM). The I–V characteristics of these junctions were measured after annealing at 400 °C for 5 min in a nitrogen ambient. In the actual process for fabricating the 3J cell [22], [23], the bonding interfaces were annealed using the same conditions.

We prepared the Si bottom cells by ion implantation to p^--Si (100) substrates and annealing. ITO films were deposited on their ∼10-nm-thick n^+ emitters. We separately prepared lattice-matched n-on-p InGaP/GaAs 2J heterostructures with p^+-GaAs bonding layers and with n^+-GaAs bonding layers by MOVPE growth on GaAs (100) substrates. n^+-GaAs/p^+-GaAs tunnel junctions were formed on top of the latter structures. We bonded each of the 2J heterostructures to the ITO films on the Si bottom cells. By using a process sequences similar to that in our previous works [23], we fabricated two types of InGaP/GaAs/ITO/Si hybrid 3J cells, 3J(a) and 3J(b), which had the p^+-GaAs/ITO and n^+-GaAs/ITO bonding interfaces, respectively. In addition, we prepared a 3J cell with a p^+-GaAs/n^+-Si bonding interface as reference [3J(c)]. Schematic cross-sections of the 3J(a), 3J(b), and 3J(c) cells are shown in Fig. 1(a), 1(b), and 1(c), respectively. The I–V characteristics in the dark as well as under air mass 1.5G/one sun irradiance were measured
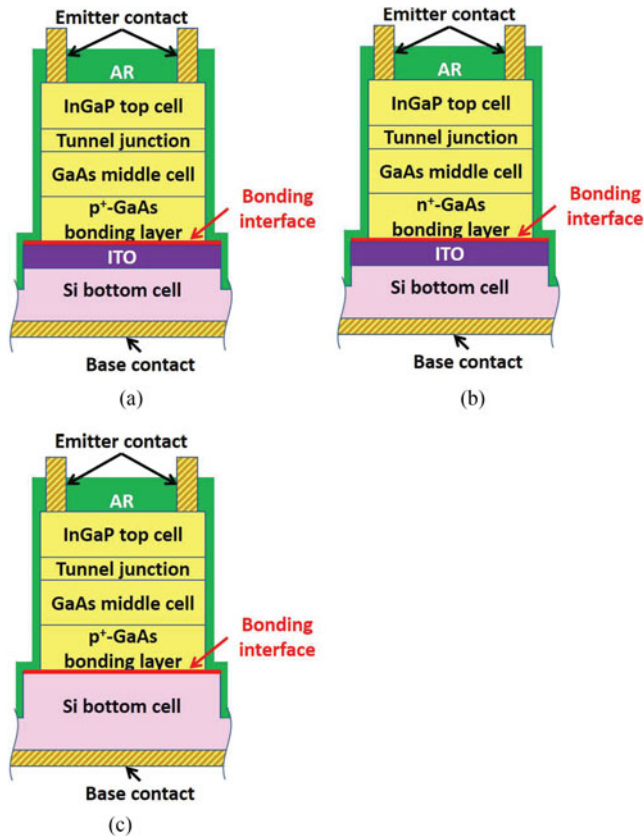
Fig. 1. Schematic cross-sections of (a) InGaP/GaAs/ITO/Si 3J cells with p^+-GaAs/ITO bonding interfaces [3J(a)], (b) InGaP/GaAs/ITO/Si 3J cells with n^+-GaAs/ITO bonding interfaces [3J(b)], and (c) InGaP/GaAs/Si 3J cells with p^+-GaAs/n^+-Si bonding interfaces [3J(c)].

for the respective 3J cells with 1-mm^2 III-V mesas using an in-house solar simulator equipped with a Xe lamp. The *I–V* characteristics under the solar irradiance were measured without masking the periphery of the Si. The external quantum efficiency (EQE) and reflectance of each 3J cell with a 2 × 2-mm III-V mesa were also measured.

B. Characterization of ITO Films and GaAs/ITO/Si Junctions

An AFM image of an ITO film is shown in Fig. 2(a). We found that the averaged roughness of the ITO surface was ≈0.3 nm, which was small enough for the ITO film to be firmly bonded using the SAB. The optical transmittance of the ITO film deposited on a glass plate is shown in Fig. 2(b). The transmittance measured after the irradiation by the FAB of Ar is also shown in this figure. The transmittance was slightly increased by the Ar beam irradiation, which was likely to be due to the slight etching of the ITO film. The reflectance of the ITO/Si (100) substrate is shown in Fig. 2(c), which also compares the measured reflectance with the calculation obtained by using a reported refractive index of the ITO film [50], which is also shown in this figure. The two curves are roughly close to each other, suggesting that the refractive index of the ITO films is ∼1.7 in the vicinity of 900 nm.

An SEM image of a GaAs/ITO/Si junction is shown in Fig. 3(a). No voids were observed at the interface, thanks to the
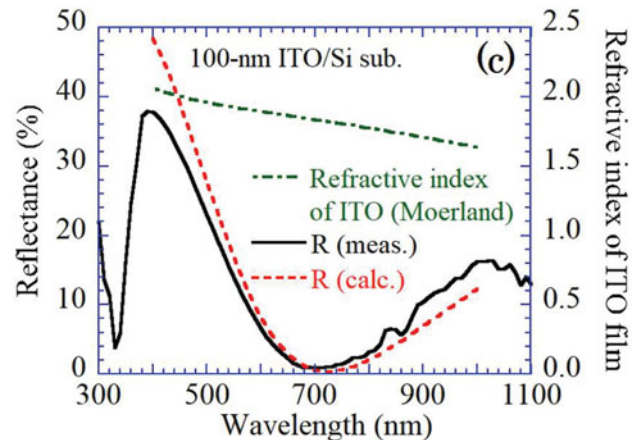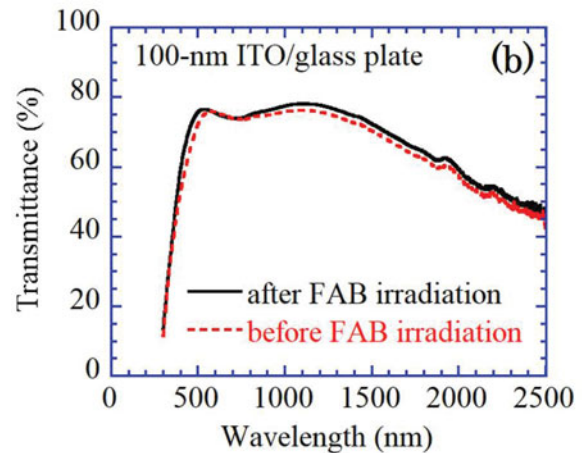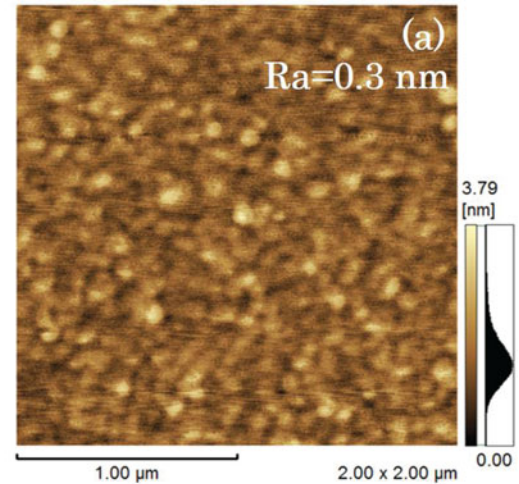
Fig. 2. (a) AFM image of an ITO film deposited on an Si substrate. (b) Optical transmittance spectra of a 100-nm-thick ITO film deposited on a glass plate. The spectrum measured after the Ar-beam irradiation is compared with that before irradiation. (c) Reflectance spectrum of a 100-nm-thick ITO film deposited on an Si (100) substrate. A comparison with a calculation using a reported refractive index of ITO [50] is also shown.

smooth surface of the ITO films. The thickness of the ITO layer was ≈100 nm as is shown in the inset. The *I–V* characteristics of the p^+-GaAs/ITO/n^+-Si and n^+-GaAs/ITO/n^+-Si junctions are shown in Fig. 3(b). The *I–V* characteristics of both junctions revealed nonohmic properties. The differential resistances in the
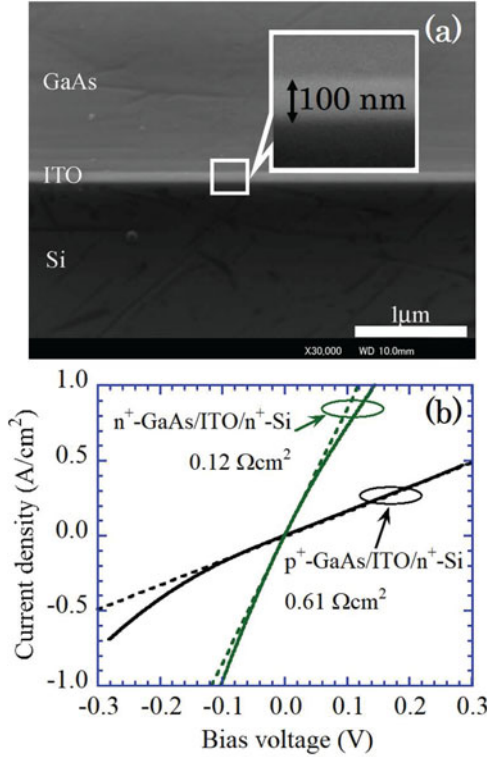
Fig. 3. (a) SEM image of a GaAs/ITO/Si junction. (b) I–V characteristics of p^+-GaAs/ITO/n^+-Si and n^+-GaAs/ITO/n^+-Si two-terminal devices after annealing at 400 °C for 5 min. The differential resistances, or the slopes of the respective I–V curves in the vicinity of 0 V, were estimated by using a least-squares fitting. The results of the fitting are shown by dashed lines.

vicinity of 0 V were estimated to be 0.61 and 0.12 Ω cm^2 for the p^+-GaAs/ITO/n^+-Si and n^+-GaAs/ITO/n^+-Si junctions, respectively, by fitting the data to straight lines. The results of the fitting are shown by dashed lines. The differential resistance of the n^+-GaAs/ITO/n^+-Si junction was slightly (1.6 times) higher than a resistance across the n^+-GaAs/n^+-Si junction (0.074 Ω cm^2 [32]). The resistance of the p^+-GaAs/ITO/n^+-Si junction was much ($\approx$5 times) higher than a resistance of the p^+-GaAs/n^+-Si junction (0.13 Ω cm^2 [31]).

C. Characterization of 3J Cells With ITO Intermediate Layers

The I–V characteristics of 3J(a), 3J(b), and 3J(c) measured in the dark are shown in Fig. 4(a). We obtained the differential resistance R_{diff} from the parts for forward-bias voltages in the respective curves. The relationships between R_{diff} and forward-bias current I_F are shown in Fig. 4(b). We found that R_{diff} was lowered by employing the ITO intermediate layers. The lowest differential resistance was obtained in 3J(b). These relationships are also shown on a log–log scale in the inset. It was found that R_{diff} in each 3J cell was almost inversely proportional to I_F. The dependence of the product of the forward current and differential resistance $I_F R_{\mathrm{diff}}$ on I_F is shown in Fig. 4(c). We found that $I_F R_{\mathrm{diff}}$ increased as I_F increased. The slopes of $I_F R_{\mathrm{diff}}$ were estimated to be $\approx$4.5, $\approx$0.02, and $\approx$7 Ωcm^2 for 3J(a), 3J(b), and 3J(c), respectively, by the least-squares fitting. It was also
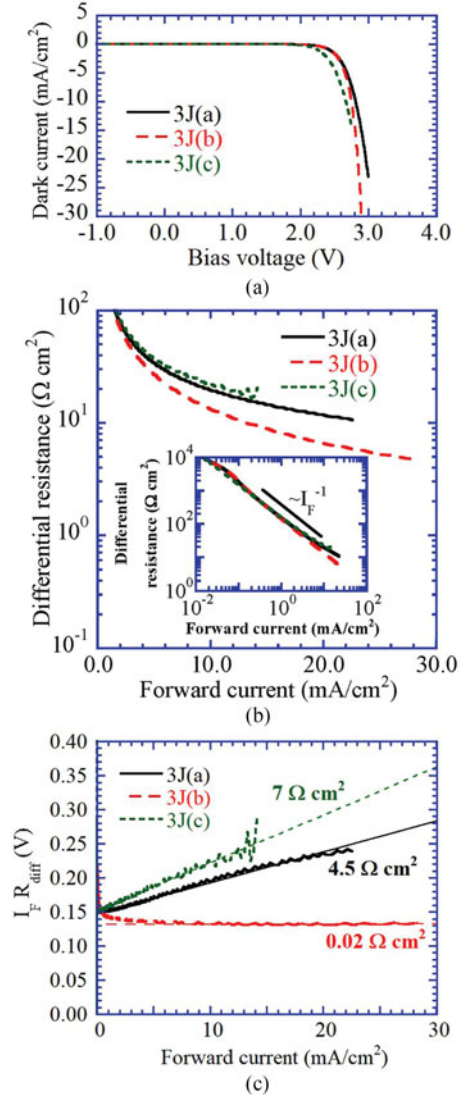
Fig. 4. (a) I–V characteristics of the 3J cells in the dark. (b) Relationships between the differential resistance and forward current of the 3J cells in the dark. The inset shows the relationships on a log–log scale. (c) Dependence of the product of the forward current and differential resistance on the forward current.

found that $I_F R_{\mathrm{diff}}$ converges to 130–150 mV at the limit of $I_F = 0$ mA/cm^2.

The EQEs of 3J(a), 3J(b), and 3J(c) are shown in Fig. 5(a), (b), and (c), respectively. The reflectance and internal quantum efficiency are also shown in each figure. The measured EQEs suggested that the short-circuit current of the 3J cell was limited by the current generated in the bottom cell. Furthermore, the EQEs of the bottom cells of 3J(a) and 3J(b) were markedly smaller than that of 3J(c), which indicated that the reflectance in 3J(a) and 3J(b) was higher than that in 3J(c) for wavelengths >900 nm. It is assumed, consequently, that the reflection at ITO films limits the performance of the bottom cell. Noting that the refractive index of the ITO film is ~1.7 for this wavelength range, the optimum thickness of the ITO film for minimizing the reflectance is estimated to be $\approx$200 nm (not depicted).
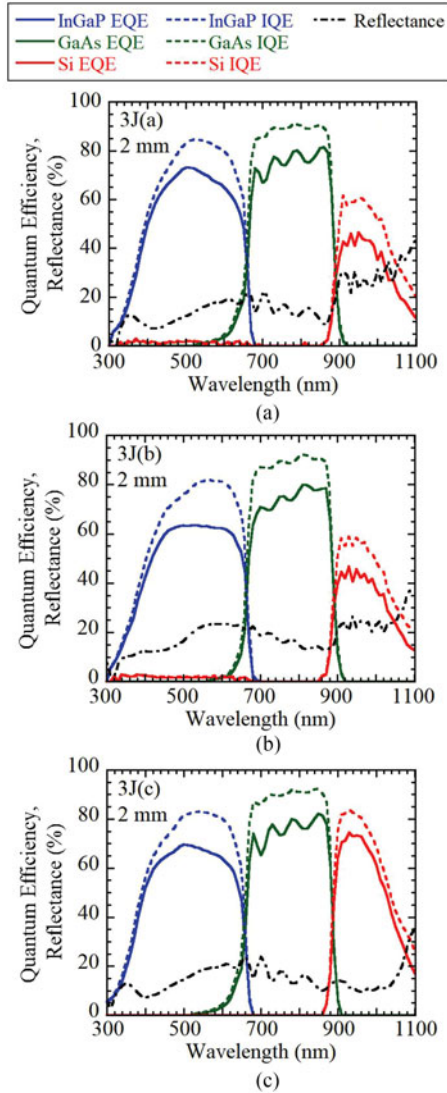
Fig. 5. Spectral responses of 2 × 2-mm (a) 3J(a), (b) 3J(b), and (c) 3J(c) cells. The external quantum efficiencies, reflectance, and internal quantum efficiencies are shown.

Fig. 6. *I–V* characteristics of (a) 3J(a), (b) 3J(b), and (c) 3J(c) cells measured under solar irradiance of AM1.5G and one sun using in-house facilities. Red straight lines show the slopes at 0 mA/cm^2 for the respective characteristics. The Si peripheries were not masked during the measurements.

The *I–V* characteristics of the 3J cells under the air mass 1.5G/one sun irradiance are shown in Fig. 6(a), (b), and (c) for 3J(a), 3J(b), and 3J(c), respectively. Values of characteristics parameters of the *I–V* curves are summarized in Table I. The short-circuit current/fill factors (FFs) of 3J(a), 3J(b), and 3J(c) were 0.106 mA/cm^2/83.4%, 0.107 mA/cm^2/85.6%, and 0.106 mA/cm^2/84.1%, respectively. The differential resistances at the open-circuit voltage ($I = 0$ mA/cm^2), which we obtained by the least-squares fitting, were 17.0, 11.3, and 18.0 Ωcm^2 for 3J(a), 3J(b), and 3J(c), respectively, as is seen from the slopes of the red straight lines in the figures. Among the three 3J cells, 3J(b) exhibited the largest FF due to its lowest resistance at $I = 0$ mA/cm^2.

Although the results of EQE measurements indicate that the short-circuit current of the 3J cell should be limited by the reflection at the ITO film, the actually measured short-circuit currents of the three 3J cells agreed with one another. This can be explained by unmasked periphery of Si in the *I–V* measurement, i.e., the Si bottom cell worked as the source of the overwhelming current in the 3J cells. The observed differential resistances at 0 mA/cm^2 were, consequently, likely to be dominated by the electrical conduction across the bonding interfaces, not by the properties of the respective subcells.

TABLE I
CHARACTERISTIC PARAMETERS OF THE FABRICATED 3J CELLS MEASURED
UNDER AIR MASS 1.5G/ONE SUN WITHOUT MASKS FOR SI PERIPHERIES

3J type	3J(a)	3J(b)	3J(c)
Short-circuit current (mA/cm^2)	10.6	10.7	10.6
Open-circuit voltage (V)	2.77	2.76	2.69
FF (%)	83.4	85.6	84.1
$- dV/dI$ @0 mA/cm^2 (Ω cm^2)	17.0	11.3	18.0

The conversion efficiencies of the fabricated 3J cells, which are 24.6 [3J(a)], 25.1 [3J(b)], and 24.0% [3J(c)], should be compared with the reported efficiency of unmasked InGaP/GaAs/Si 3J cells (27.2% for the air mass 1.5D/one sun irradiance [24]). The difference might be because of the open-circuit voltage in the bottom cells.

III. DISCUSSION

Two interfaces (GaAs/ITO and ITO/Si) are formed by placing the ITO layers between heavily doped GaAs and Si. Each of the newly formed interfaces might cause an additional resistance. In contrast, the ITO layer itself is expected to play a role in lowering the interface resistance since its electron concentration is higher than the concentrations in conventional n-type semiconductors. The difference in the resistance between the junctions with and without ITO intermediate layers is likely to be the result of such a tradeoff.

The I–V characteristics of p–n junctions in the dark for forward-bias voltages are approximately expressed as $I_F \approx I_0 \exp(qV/nk_BT)$, where I_0, q, n, k_B, and T are the saturation current density, the elementary charge, the ideality factor of the p–n junctions, Boltzmann constant, and the lattice temperature (300 K), respectively. Then, the differential resistance of single p–n diodes for forward-bias voltages, or the intrinsic resistance of p–n diodes, is expressed as nk_BT/qI_F for $I_F >> I_0$. Consequently the differential resistance of the 3J cells is approximately given by

$$R_{\text{diff}} = \frac{(n_1 + n_2 + n_3)k_BT}{qI_F} + R_{\text{para}} \qquad (1)$$

where n_1, n_2, and n_3 are the ideality factors of the p–n junctions in the top, middle, and bottom cells, respectively. R_{para} stands for the parasitic resistance in the dark, which is attributed to resistances in the contacts at the emitter and base, the semiconductor substrates, tunnel junctions, and bonding interfaces. We obtain from the above equation

$$\lim_{I_F \to 0} I_F R_{\text{diff}} = \frac{(n_1 + n_2 + n_3)k_BT}{q} \qquad (2)$$

and

$$\frac{\partial I_F R_{\text{diff}}}{\partial I_F} = R_{\text{para}}. \qquad (3)$$

The usage of (1) is justified by that the measured differential resistance was almost inversely proportional to the forward-bias current [inset of Fig. 4(b)]. Based on (2), that the zero-current limit value of $I_F R_{\text{diff}}$ was 130–150 mV [see Fig. 4(c)] means that $n_1 + n_2 + n_3 \approx 5$–5.8, which fulfills the requirement for the ideality factors ($1 < n_1, n_2, n_3 < 2$).

Using (3), we find that the R_{para} values in 3J(a), 3J(b), 3J(c) are ~4.5, ~0.02, and ~7 $\Omega \cdot$cm^2, respectively, from the respective curves in Fig. 4(c). R_{para} in 3J(c) is the largest among the three 3J cells. In contrast, R_{para} in 3J(b) is negligibly small. The R_{para} values in 3J(a) and 3J(c) are likely to be dominated by the resistance at GaAs/ITO/Si and GaAs/Si junctions, respectively, since the process relevant to the other parts of the parasitic resistance is the same among the three 3J cells.

R_{para} for 3J(c) should be comparable to the interface resistance estimated for actual 3J cells with p^+-GaAs/n^+-Si bonding interfaces (several Ω cm^2 as stated above [42]). The lower R_{para} for 3J(a) and 3J(b) is attributed to the evaporated ITO films that played a role in effectively enhancing the thickness of the bonding layers of the bottom cell. Noting that the electrical conduction is likely to be influenced by the interface states formed in the vicinity of the bonding interface [27], the deposited ITO films can protect the underlying semiconductor layers, n^+-Si emitters in the present case, from the damage because of the SAB process.

The smaller R_{para} in 3J(b) compared with that in 3J(a) is consistent with the result that the resistance in the n^+-GaAs/ITO/n^+-Si junction was lower than that in the p^+-GaAs/ITO/n^+-Si junction [see Fig. 3(b)].

The contribution of the intrinsic resistance of 3J cells to the differential resistance at 0 mA/cm^2 under the solar irradiance is approximately given by $(n_1 + n_2 + n_3)k_BT/(qI_{\text{SC}})$ with the short-circuit current I_{SC}. For the investigated 3J cells, this value should amount to $12 \sim 14 \, \Omega \cdot$cm^2 since $n_1 + n_2 + n_3 \approx 5$–5.8. The differential resistance obtained for 3J(b) under the solar irradiance, 11.3 $\Omega \cdot$cm^2 as is shown in Table I, is close to this estimation. This means that the differential resistance under the solar irradiance was dominated by the intrinsic resistance for 3J(b). This contention is supported by the result that R_{para} in 3J(b) was the smallest among the three 3J cells, which was the origin of its highest FF.

The results of the present work suggest that n^+-GaAs/ITO/n^+-Si junctions with GaAs/ITO bonding interfaces are likely to be promising for achieving better performances in hybrid multijunction cells. We have to note, however, that the obtained R_{para} in 3J(b) is still high in comparison with the reported resistance of bonding interfaces in n^+-GaAs/n^+-Si junctions [41]. Although R_{para} in the present work was estimated for junctions made of layers with finite thicknesses, i.e., not for junctions of heavily doped substrates, one possible explanation is that differences in the SAB process conditions such as the treatment of sample surfaces before bonding and the acceleration voltage of the FAB play a dominant role. If such an explanation is acceptable, a further decrease in R_{para} might be achieved by combining the approach in the present work with optimization of the SAB conditions.

IV. CONCLUSION

By applying SAB technologies, we successfully fabricated an InGaP/GaAs/ITO/Si 3J cell with a p^+-GaAs/ITO/n^+-Si junction and a 3J cell with an n^+-GaAs/ITO/n^+-Si junction. The characteristics of these 3J cells were compared with those of a conventional InGaP/GaAs/Si 3J cell with a p^+-GaAs/n^+-Si junction. By analyzing the characteristics in the dark, the parasitic resistances, or the parasitic parts in the differential resistances, of the respective 3J cells were distinguished from the intrinsic parts, which were proportional to the ideality factors of subcells. Among the three 3J cells, the cell with an n^+-GaAs/ITO/n^+-Si junction showed the lowest parasitic resistance. The observed resistance was negligibly small in

comparison with the other two 3J cells. This finding was in accordance with measurements of the characteristics of the 3J cells under solar irradiance, which indicated that, among the investigated 3J cells, the differential resistance at 0 mA/cm^2 was the lowest and FF was the largest for the cell with an n^+-GaAs/ITO/n^+-Si junction. The obtained results indicated that the performances of III-V-on-Si multijunction cells can be improved by utilizing n^+-GaAs/ITO/n^+-Si junctions in combination with the optimization of the SAB process.

ACKNOWLEDGMENT

REFERENCES

[1] M. A. Green *et al.*, "Solar cell efficiency tables (version 50)," *Prog. Photovolt. Res. Appl.*, vol. 25, pp. 668–676, 2017.

[2] H. Sugiura, C. Amano, A. Yamamoto, and M. Yamaguchi, "Double heterostructure GaAs tunnel junction for a AlGaAs/GaAs tandem solar cell," *Jpn. J. Appl. Phys.*, vol. 27, pp. 269–272, 1988.

[3] J. M. Olson, S. R. Kurtz, A. E. Kibbler, and P. Faine, "A 27.3% efficient Ga0.5In0.5P/GaAs tandem solar cell," *Appl. Phys. Lett.*, vol. 56, pp. 623–625, 1990.

[4] K. A. Bertness *et al.*, "29.5%-efficient GaInP/GaAs tandem solar cells," *Appl. Phys. Lett.*, vol. 65, pp. 989–991, 1994.

[5] T. Takamoto, E. Ikeda, and H. Kurita, "Over 30% efficient InGaP/GaAs tandem solar cells," *Appl. Phys. Lett.*, vol. 70, pp. 381–383, 1997.

[6] T. Takamoto *et al.*, "Two-terminal monolithic In$_{0.5}$ Ga$_{0.5}$ P/GaAs tandem solar cells with a high conversion efficiency of over 30%," *Jpn. J. Appl. Phys.*, vol. 36, pp. 6215–6220, 1997.

[7] T. Takamoto, M. Kaneiwa, M. Imaizumi, and M. Yamaguchi, "InGaP/GaAs-based multijunction solar cells," *Prog. Photovolt: Res. Appl.*, vol. 13, pp. 495–511, 2005.

[8] J. F. Geisz *et al.*, "High-efficiency GaInP/GaAs/InGaAs triple-junction solar cells grown inverted with a metamorphic bottom junction," *Appl. Phys. Lett.*, vol. 91, pp. 023502-1–023502-3, 2007.

[9] F. Dimroth *et al.*, "Wafer bonded four-junction GaInP/GaAs//GaInAsP/GaInAs concentrator solar cells with 44.7% efficiency," *Prog. Photovolt: Res. Appl.*, vol. 22, pp. 277–282, 2014.

[10] F. Dimroth *et al.*, "Four-Junction wafer-bonded concentrator solar cells," *IEEE J. Photovolt.*, vol. 6, no. 1, pp. 343–349, Jan. 2016.

[11] D. C. Bobela, L. Gedvilas, M. Woodhouse, K. A. W. Horowitz, and P. A. Basore, "Economic competitiveness of III-V on silicon tandem one-sun photovoltaic solar modules in favorable future scenarios," *Prog. Photovolt. Res. Appl.*, vol. 25, pp. 41–48, 2017.

[12] T. Soga, K. Baskar, T. Kato, T. Jimbo, and M. Umeno, "MOCVD growth of high efficiency current-matched AlGaAs/Si tandem solar cell," *J. Crystal Growth*, vol. 174, pp. 579–584, 1997.

[13] F. Dimroth *et al.*, "Comparison of direct growth and wafer bonding for the fabrication of GaInP/GaAs dual-junction solar cells on silicon," *IEEE J. Photovolt.*, vol. 4, no. 2, pp. 620–625, Mar. 2014.

[14] T. J. Grassman *et al.*, "Characterization of metamorphic GaAsP/Si materials and devices for photovoltaic application," *IEEE Trans. Electron Devices*, vol. 57, no. 12, pp. 3361–3369, Dec. 2010.

[15] M. R. Lueck *et al.*, "Dual junction GaInP/GaAs solar cells grown on metamorphic SiGe/Si substrates with high open circuit voltage," *IEEE Electron Device Lett.*, vol. 27, no. 3, pp. 142–144, Mar. 2006.

[16] M. J. Archer *et al.*, "GaInP/GaAs dual junction solar cells on Ge/Si epitaxial templates," *Appl. Phys. Lett.*, vol. 92, pp. 103503-1–103503-3, 2008.

[17] O. Moutanabbir and U. Gösele, "Heterogeneous integration of compound semiconductors," *Annu. Rev. Mater. Res.*, vol. 40, pp. 469–500, 2010.

[18] K. Tanabe, K. Watanabe, and Y. Arakawa, "III-V/Si hybrid photonic devices by direct fusion bonding," *Sci. Rep.*, vol. 2, pp. 349-1–349-6, 2012.

[19] K. Tanabe, A. F. I. Morral, H. A. Atwater, D. J. Aiken, and M. W. Wanlass, "Direct-bonded GaAs/InGaAs tandem solar cell," *Appl. Phys. Lett.*, vol. 89, pp. 102106-1–102106-3, 2006.

[20] H. Mizuno *et al.*, "High-efficiency III-V//Si tandem solar cells enabled by the Pd nanoparticle array-mediated gsmart stackh approach," *Appl. Phys. Express*, vol. 10, pp. 072301-1–072301-4, 2017.

[21] K. Derendorf *et al.*, "Fabrication of GaInP/GaAs//Si solar cells by surface activated direct wafer bonding," *IEEE J. Photovolt.*, vol. 3, no. 4, pp. 1423–1428, Oct. 2013.

[22] N. Shigekawa, M. Morimoto, S. Nishida, and J. Liang, "Surface-activated-bonding-based InGaP-on-Si double-junction cells," *Jpn. J. Appl. Phys.*, vol. 53, pp. 04ER05-1–04ER05-4, 2014.

[23] N. Shigekawa *et al.*, "Current-voltage and spectral-response characteristics of surface-activated-bonding-based InGaP/GaAs/Si hybrid triple-junction cells," *Jpn. J. Appl. Phys.*, vol. 54, pp. 08KE03-1–08KE03-5, 2015.

[24] S. Essig *et al.*, "Wafer-bonded GaInP/GaAs//Si solar cells with 30% efficiency under concentrated sunlight," *IEEE J. Photovolt.*, vol. 5, no. 3, pp. 977–981, May 2015.

[25] H. Takagi, K. Kikuchi, R. Maeda, T. R. Chung, and T. Suga, "Surface activated bonding of silicon wafers at room temperature," *Appl. Phys. Lett.*, vol. 68, pp. 2222–2224, 1996.

[26] J. Liang, T. Miyazaki, M. Morimoto, S. Nishida, and N. Shigekawa, "Electrical properties of Si/Si interfaces by using surface-activated bonding," *J. Appl. Phys.*, vol. 114, pp. 183703-1–183703-6, 2014.

[27] M. Morimoto, J. Liang, S. Nishida, and N. Shigekawa, "Effects of annealing on electrical properties of Si/Si junctions by surface-activated bonding," *Jpn. J. Appl. Phys.*, vol. 54, pp. 030212-1–030212-5, 2015.

[28] K. Watanabe *et al.*, "Microscopy and electrical properties of Ge/Ge interfaces bonded by surface-activated wafer bonding technology," *Jpn. J. Appl. Phys.*, vol. 50, pp. 015701-1–015701-5, 2011.

[29] M. M. R. Howlader, T. Watanabe, and T. Suga, "Investigation of the bonding strength and interface current of p-Si/n-GaAs wafers bonded by surface activated bonding at room temperature," *J. Vac. Sci. Technol. B*, vol. 19, no. 6, pp. 2114–2118, 2001.

[30] J. Liang *et al.*, "Electrical properties of p-Si/n-GaAs heterojunctions by using surface-activated bonding," *Appl. Phys. Express*, vol. 6, pp. 021801-1–021801-3, 2013.

[31] J. Liang, S. Nishida, M. Morimoto, and N. Shigekawa, "Surface-activating-bonding-based low-resistance Si/III-V junctions," *Electron. Lett.*, vol. 49, pp. 830–832, 2013.

[32] J. Liang, L. Chai, S. Nishida, M. Morimoto, and N. Shigekawa, "Investigation on the interface resistance of Si/GaAs heterojunctions fabricated by surface-activated bonding," *Jpn. J. Appl. Phys.*, vol. 54, pp. 030211-1–030211-5, 2015.

[33] M. M. R. Howlader, T. Watanabe, and T. Suga, "Characterization of the bonding strength and interface current of p-Si/n-InP wafers bonded by surface activated bonding method at room temperature," *J. Appl. Phys.*, vol. 91, pp. 3062–3066, 2002.

[34] J. Liang, M. Morimoto, S. Nishida, and N. Shigekawa, "Band structures of Si/InGaP heterojunctions by using surface-activated bonding," *Phys. Status Solidi C*, vol. 10, pp. 1644–1647, 2013.

[35] N. Shigekawa, N. Watanabe, and E. Higurashi, "Electrical properties of si-based junctions by SAB," in *Proc. 3rd Int. IEEE Workshop Low Temperature Bonding 3D Integr.*, 2012, pp. 109–112.

[36] J. Liang, S. Nishida, M. Arai, and N. Shigekawa, "Effects of thermal annealing process on the electrical properties of p$^+$-Si/n-SiC heterojunctions," *Appl. Phys. Lett.*, vol. 104, pp. 161604-1–161604-4, 2014.

[37] J. Liang, S. Nishida, T. Hayashi, M. Arai, and N. Shigekawa, "Effects of interface state charges on the electrical properties of Si/SiC heterojunctions," *Appl. Phys. Lett.*, vol. 105, pp. 151607-1–151607-4, 2014.

[38] R. Cariou *et al.*, "Monolithic two-terminal III-V//Si triple-junction solar cells with 30.2% efficiency under 1-Sun AM1.5g," *IEEE J. Photovolt.*, vol. 7, no. 1, pp. 367–373, Jan. 2017.

[39] T. Tayagaki, K. Makita, H. Mizuno, R. Oshima, and T. Sugaya, "Investigation of the open-circuit voltage in mechanically stacked InGaP/GaAs//InGaAsP/InGaAs solar cells," *Jpn. J. Appl. Phys.*, vol. 56, pp. 08MC01-1–08MC01-5, 2017.

[40] Z. Ren *et al.*, "The GaAs/GaAs/Si solar cell—Towards current matching in an integrated two terminal tandem," *Sol. Energy Mater. Sol. Cells*, vol. 160, pp. 94–100, 2017.

[41] S. Essig and F. Dimroth, "Fast atom beam activated wafer bonds between n-Si and n-GaAs with low resistance," *ECS J. Solid State Sci. Technol.*, vol. 2, pp. Q178–Q181, 2013.

[42] N. Shigekawa and J. Liang, "Impacts of bonding-layer resistance of Si bottom cells on interface resistance in InGaP/GaAs/Si hybrid triple-junction cells," in *Proc. 5th Int. Workshop Low Temperature Bonding 3D Integr.*, 2017, p. 52.

[43] J. B. DuBow, D. E. Burk, and J. R. Sites, "Efficient photovoltaic heterojunctions of indium tin oxides on silicon," *Appl. Phys. Lett.*, vol. 29, pp. 494–496, 1976.
[44] B. Parida, H. Y. Ji, G. H. Lim, S. Park, and K. Kim, "Enhanced photocurrent of Si solar cell with the inclusion of a transparent indium tin oxide thin film," *J. Renewable Sustain. Energy*, vol. 6, pp. 053120-1–053120-8, 2014.
[45] H. W. Du *et al.*, "The bifunctional tin-doped indium oxide as hole-selective contact and collector in silicon heterojunction solar cell with a stable intermediate oxide layer," *Solar Energy*, vol. 155, pp. 963–970, 2017.
[46] Y.-C. Kao, S.-L. Ou, F.-L. Wu, and R.-H. Horng, "Performance enhancement of III-V multi-junction solar cells using indium-tin-oxide electrodes," *Thin Solid Films*, vol. 612, pp. 36–40, 2016.
[47] P.-C. Liu, C.-Y. Hou, and Y.-S. Wu, "Wafer bonding for high-brightness light-emitting diodes via indium tin oxide intermediate layers," *Thin Solid Films*, vol. 478, pp. 280–285, 2005.
[48] J. Liang *et al.*, "Electrical conduction of Si/ITO/Si junctions fabricated by surface activated bonding," *Jpn. J. Appl. Phys.*, vol. 57, pp. 02BE03-1–02BE03-5, 2018.
[49] N. Shigekawa *et al.*, "InGaP/GaAs/ITO/Si hybrid triple-junction cells with GaAs/ITO bonding interfaces," presented at the 2017 IEEE Photovolt. Energy Convers., Washington, DC, USA, Jun. 25–30, 2017, Paper I35.
[50] R. J. Moerland and J. P. Hoogenboom, "Subnanometer-accuracy optical distance ruler based on fluorescence quenching by transparent conductors: supplementary material," *Optica*, vol. 3, pp. 112–117, 2016.
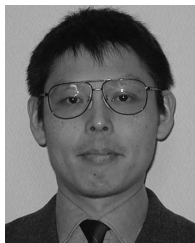
Naoteru Shigekawa (M'01) received the B.S., M.S., and Ph.D. degrees in physics from the University of Tokyo, Tokyo, Japan, in 1984, 1986, and 1993, respectively.

He was with the Nippon Telegraph and Telephone (NTT) Laboratories, NTT Corporation, Atsugi, Japan, between 1986 and 2011. He was engaged in research on hot-carrier transport in III-V compound-semiconductor heterostructures and electron devices at NTT Laboratories. From 1993 to 1994, he was a Visiting Scientist with the Department of Physics, University of Nottingham, Nottingham, U.K. Since 2011, he has been with the Graduate School of Engineering, Osaka City University, Osaka, Japan, as a Professor. His current research interest includes fabrication of heterointerfaces and advanced hybrid semiconductor devices such as multijunction solar cells and heterojunction bipolar transistors using surface activated bonding and their characterization.

Prof. Shigekawa is a member of the Physical Society of Japan, the Japan Society of Applied Physics, the Electrochemical Society, and the Institute of Physics.

Tomoya Hara received the B.Eng. degree in applied physics and electronics from Osaka City University, Osaka, Japan, in 2017. He is currently working toward the M.Eng. degree with the Graduate School of Engineering in Osaka City University.

His research interest includes surface-activated bonding for fabricating III-V-on-Si multijunction solar cells.

Jianbo Liang (M'15) was born in Hubei Province, China, in 1980. He received the M.S. and Ph.D. degrees in material engineering from the Nagoya Institute Technology, Nagoya, Japan, in 2009 and 2012, respectively.

From 2012 to 2015, he was a Postdoctoral Fellow with the Power Electrics Laboratory, Osaka City University. Since 2015, he has been a Lecturer with Osaka City University, Osaka, Japan. He was a Visiting Researcher with the University of Bristol, Bristol, U.K., in 2017. He is currently engaged in the direct bonding of various semiconductor materials for realizing advanced electronic devices and multijunction solar cells on Si substrates.

Takefumi Kamioka (M'13) received the Ph.D. degree in engineering from Waseda University, Tokyo, Japan, in 2009.

He worked on the carrier transport mechanism in nanoscale transistors by means of a molecular dynamics-based simulation as a Postdoc Researcher. Since 2014, he has been with Toyota Technological Institute, Nagoya, Japan, where he is working on the development of crystalline Si heterojunction solar cells. His current research interests include device physics that includes the modeling, simulation, and characterization of the related devices.

Kenji Araki (M'16) was born in Nagoya, Japan, in 1960. He received the B.S. degree in electronics engineering from Kyoto University, Kyoto, Japan, in 1984 and the Ph.D. degree in engineering from Nagoya Institute of Technology, Nagoya, Japan, in 2006.

He started CPV research and development with Toyota Technological Institute in 1998 and in Daido Steel in 2000. He is an Invited Research Fellow with Toyota Technological Institute, Nagoya, Japan, and does research on CPV technology, car-roof PV, and III-V on Si cell. He has published more than 150 research items in scientific journals and international conferences. He was the Chairman of Conference of CPV-9 International Conference on CPV Technology in 2012, and he is a convenor of the IEC TC82 working group 7 focused on the development of international standards related to CPV and solar trackers.

Masafumi Yamaguchi (LM'87) was born in Hokkaido, Japan, in 1946. He received the B.S. and Ph.D. degrees from Hokkaido University, Sapporo, Japan, in 1968 and 1978, respectively.

He is currently a Professor Emeritus and Senior Research Scholar with the Toyota Technological Institute, Nagoya, Japan. He found superior radiation-resistance of InP-related materials and solar cells and his group contributed to the development of high-efficiency III-V compound multijunction, space, and concentrator solar cells. He led Japanese National PV Programs as the Project Leader of the NEDO Project and the Research Supervisor of the JST Program.

Prof. Yamaguchi has received several awards such as the Becquerel Prize from the European Commission in 2004, the William Cherry Award from the IEEE in 2008, the PVSEC Award in 2011, and the WCPEC Award in 2014 for his outstanding contributions to the development of science and technology of photovoltaics and as one of the world leaders of the development of photovoltaics and as one of the driving forces for international collaboration and cooperation.

Tomoki Ogawa, photograph and biography not available at the time of publication.